Buckling of fibres and yarns within ropes and other fibre assemblies

R.E. Hobbs*, M.S. Overington, J.W.S. Hearle and S.J. Banfield

Tension Technology International Ltd, TTI House, Preston PR1 3NA, UK

* Address for correspondence: Department of Civil Engineering, Imperial College, London SW7 2BU, UK

Individual yarns within ropes can be subject to axial compression even though the rope as a whole is under tension. This leads to buckling in sharp kinks and then to failure by axial compression fatigue after repeated cycling. An existing elastic theory, which applies to heated pipelines subject to lateral and axial restraint, predicts alternative modes of either continuous buckling or intermittent buckled zones alternating with slip zones. The mechanics of axially compressed yarns within ropes are similar, but the theory has been extended to cover plastic deformation at hinge points. The predicted form of groups of saw-tooth buckles, which curve at the ends of the zones into the slip lengths, is in agreement with observed effects. Numerical calculation gives quantitative predictions in agreement with experimental results, despite uncertainty about the correct values for bending stiffness and plastic yield moment, depending on whether the yarns act as solid rods or freely slipping fibre assemblies.

1 INTRODUCTION

Fibre and wire ropes are primarily intended for service as tensile elements, but failure may result from axial compression of parts of the cross-section, namely individual fibres, yarns or strands, while the bulk of the rope is safely in tension. Similar effects may occur in other textile structures, such as carpets or industrial woven fabrics. If the axial compression leads to a mild rounded buckling, as in an elastic deformation, there will be little damage, but if, as often happens, plastic yielding leads to sharp kinks, then fibres will fail in repeated cycling. In ropes, axial compression of individual components can arise from a number of causes including:

C   Bending. If a rope under tension passes over a sheave (pulley) or is taken round any other solid object with too small a radius, components inside the curve may be put into compression. Ropes may also buckle into bent forms or, at low or zero tension, be forced to bend by transverse forces.

C   Rope twisting. If a parallel assembly of fibres is twisted in either direction at constant length, the outer layers are forced into longer paths and so develop tension. If the overall rope tension falls below the value developed in this way, the rope will contract and the central fibres will be put into compression. In a simple twisted structure, an increase of twist will cause the central straight components to go into compression, whereas a decrease of twist will compress the outer components. In more complicated rope structures, with twist at several levels, the precise effects will depend on the geometry, but twisting will always force some components into axial compression in the absence of sufficient overall rope tension.

Twisting in tension-tension cycling can develop for two reasons. If the rope is not torque-balanced, tension will cause a torque to develop, and this can lead to the rope twisting against a soft termination, such as a splice, or against other line components. Similarly, if other line components, such as connecting wire ropes, are not torque-balanced, twist may be transmitted to the fibre rope. Alternatively, if there is nonuniformity along the rope, different sections of rope will twist against each other. All of these effects have been found in practice.

Buckling into three-dimensional curved paths also gives rise to twist.

C   Length imbalance. If, as a result of manufacture or subsequent handling and use, one or more components of a rope is longer (parallel to the axis of the rope) at zero tension than the other components, then the equilibrium state of the entire rope at zero tension will have the longer components in compression and the shorter ones in tension. A critical positive tension is needed to eliminate axial compression in the longer elements.

Similar effects can clearly arise in umbilicals, armoured electrical and optical cables, and hoses. Indeed, the wider range of elemental properties in some of these products may make sensitive elements such as optical fibres more rather than less likely to be put into compression.

Compression by itself is not usually a major problem, rather it is the response to compression, and how often this response is repeated which is of concern. If a rope as a whole is subject to an axial compressive force, it will buckle into a smooth curve with a radius that is too large to cause fibre damage. The only exceptions would be for very short lengths of rope or where a rope is restrained from buckling by a lateral pressure. The common damaging situation is when a component within a rope is forced into compression while subject to the restraint of neighbouring components, such as a sheave, or other rope components which are still under tension. In high strength fibre ropes, this restrained buckling of the compressed element is known as kinking, and is a form of elasto-plastic buckling of the fibre or group of fibres against the restraint afforded by the neighbouring elements which are still in tension.

Kinking due to axial compression is a phenomenon that occurs on many scales from mountain ranges to oriented polymer molecules. In fibres, the effects at the molecular level are shown by the presence of kinkbands, which run across the fibres at about 45E, when fibres are uniformly compressed, or, more commonly, on the inside of bends. Repeated flexing of fibres leads to failure, either due to breakdown along kinkbands or to axial splitting from the accompanying shear stresses. As described by Hearle et al (1998), these forms of failure have been observed in laboratory flex tests and in ropes and carpets after cyclic loading. In typical test conditions, failure may occur in around 1000 cycles in aramid fibres, Hearle and Wong (1977), but polyester and nylon fibres would last longer, Hearle and Miraftab (1991). Data from yarn buckling tests carried out for FIBRE TETHERS 2000 (1995), show severe strength loss in aramid yarns after 20,000 cycles, in HMPE yarns after 200,000 cycles and in polyester yarns after 1,000,000 cycles.

The first reported engineering failure in an aramid rope due to axial compression fatigue was

in the mooring lines for the construction ship Ocean Builder I used in the erection of the Lena tower in the Gulf of Mexico in 1983, Riewald (1986) and Riewald et al (1986). The lines were deployed on buoys in 1045 feet of water 4-6 weeks before the arrival of the ship. On recovering and tensioning, four ropes failed, reportedly at 20% of rated strength. The failure was very thoroughly investigated and explained in the following way. Torque generated in the ropes due to wave action led to rotation, causing shear and compressive strains, which in turn led to fibre kinking with an accompanying loss of strength. Laboratory studies and ocean deployments, resulting from the investigation of this failure, gave more examples of kinking occurring due to axial compression. Gross kinks were seen in yarns and severe fibre damage was shown up as strongly dyed bands at regular intervals along the yarns. The study of this failure led to improved rope constructions and procedures as a way of avoiding axial compression fatigue.

The occurrence of axial compression fatigue in various types of fibre ropes was found after tension-tension cycling in the joint industry study, FIBRE TETHERS 2000 (1995). Samples of these ropes were made available for microscopic examination in the Department of Textiles at UMIST, with results reported by Hearle et al (1998). The observed effects included the following :

C   a wavy buckling of yarns or strands, at fairly low curvature, which would not be likely to cause serious damage to fibres

C   kinkbands running across fibres indicating regions of uniform axial compression

C   sharp kinks of fibres as a whole, usually occurring cooperatively across yarns

C   breaks of fibres along kinkbands within fibres

C   axial splits, which would have been caused by fibre bending

Commonly, the sharp fibre kinks, with internal damage that could be picked out by dyeing aramid yarns, occurred in groups in zig-zag sections separated by straight lengths. This, in turn, led to broken pieces, which were a few millimetres in length, followed by unbroken portions, which were a few centimetres long. Some examples are described later in this paper.

2. ANALYSIS

2.1 Approach to modelling

The observed failure modes in a rope suggest that an element of a rope fails by buckling because it is carrying an axial compressive load even though it is laterally restrained by adjacent elements carrying tension. The phenomena appear at a number of different scales in a rope : a sub-rope may buckle in a multi-rope assembly, a strand may buckle while restrained by adjacent strands, or a yarn fail when restrained by adjacent yarns. It is also observed that the buckles become more severe as the elements get smaller. Ropes and strands take up gentle, harmless elastic curves, while yarns and particularly the individual

filaments in them form much more deleterious plastic hinges or kinks, kinks which are apparent even at the molecular level. This part of the paper models the buckling of the element by examining the theory behind the buckling of a semi-infinite beam-column carrying an axial load whilst laterally supported by other elements. The beam is assumed to be elastic initially, and then to yield at a known "plastic hinge" moment. Two classes of buckles are considered, namely general periodic modes and localised modes, which are more damaging in practice because of energy inputs from adjacent, unbuckled, areas of the beam. The elastic behaviour of such a beam is, fortunately, fairly well understood because it has proved to be of economic importance in many other areas. The plastic behaviour has not, apparently, been examined before, and it is developed *ab initio* here, based on the premise that it is preceded by elastic buckling, which may be non-damaging in itself but which triggers the plastic buckling.

2.2 Elastic Buckling

As noted above, there is a large volume of earlier work on the lateral buckling of long beams against lateral restraint, related to the lateral buckling of railway tracks and, later, submarine pipelines. The lateral restraining force may be elastic, i.e. proportional to the lateral displacement, or frictional, i.e. of constant magnitude and opposing further growth of deflection.

However, for a linearly elastic lateral restraint only a periodic mode (Mode 4 of Fig.1) is possible, and the observed presence of localised modes in ropes suggests that the "frictional" or constant force lateral restraint model, where localised modes (Modes 1-4 of Fig.1) are possible, is a better choice. This view is reinforced by the presence of a radial pressure p on the buckling element in a rope under tension due to the helical nature of adjacent elements or any braided jacket. This pressure is, to the first order, unaffected by any buckle, and the lateral restraint on unit length of the element is therefore taken as pd, where d is the diameter of the element. The analysis that follows is then very close to that for submarine pipelines by Hobbs (1984) and Hobbs and Liang (1989), so that it is only presented in summary here.

In the notation of Fig.2, the governing differential equation for the buckled beam is

$$y^{))} \% n^2 y \% \frac{m}{8} (4x^2 \& L^2) \' 0 \tag{1}$$

where a prime denotes differentiation of the displacement y with respect to the longitudinal coordinate x, $m=pd/EI$ and $n^2=P/EI$. E is Young's Modulus for the beam, I its effective second moment of area, P the compressive axial load and L the buckle half-wavelength. The solution to this differential equation is presented in Hobbs (1984), but proceeds by considering the boundary conditions for the various modes, whether localised or periodic, and in each case gives a relationship of the form:

$$P \' f(L) \tag{2}$$

The other important element in the analysis is to recognise that as the buckle forms the force in it drops to maintain displacement compatibility. In the pipeline analysis, and with equal validity here, the axial load is displacement controlled rather than force controlled. In the pipeline the axial force is induced by the restraint of thermal expansion, and if (by buckling) the line can take up a slightly longer path the force will be reduced to some extent. Likewise, in the rope the compressive force will be reduced by buckling. Considering the 4 mode first, if the force just before buckling is P_o, and falls to P on buckling, displacement compatibility for a buckle of length L requires the change in arc length around the buckle to match the growth in length due to the force change, or:

$$\int_0^L \frac{1}{2}(y')^2 = (P_o - P)\frac{L}{EA} \tag{3}$$

where A is the cross-sectional area of the beam.

Using the solution to the differential equation (1), the integral on the left hand side can be evaluated and equation (3) rearranged to yield an equation of form:

$$P_o = P + g(L) \tag{4}$$

Turning to the localised modes, Modes 1-4, equations (2) and (3) will be modified by two factors. The first is trivial, in that the total length $\overline{L}$ (measured over the 1 to 4 halfwaves as appropriate) of the buckle should be considered. The second is more basic, and recognises that the compatibility condition, equation (3), should be modified to include the influence of two 'slipping lengths' adjacent to the localised buckle (Fig.3). The slip lengths form to accommodate the difference between P_o, the force remote from the buckle which is unchanged by the formation of the buckle, and the lower force P, within the buckle itself. The slip length, L_s, is determined by the effective friction between the beam and the surroundings. If the friction coefficient is μ, and the radial pressure p on a beam of diameter d, or perimeter πd, then:

$$L_s = (P_o - P)/(\mu p \pi d) \tag{5}$$

The slip lengths on either side of the buckle then feed some displacement into the buckle, equal to the average force change in L_s times the length divided by the axial rigidity. The inward movement s each side is thus:

$$s = 0.5(P_o - P) L_s/EA \tag{6}$$

The compatibility condition, equation (3) becomes:

$$\underset{m}{\overset{\bar{L}}{}}\frac{1}{2}(y')^2 \quad ' \quad (P_o \ \& \ P)\frac{\bar{L}}{EA} \quad \% \ 2s$$

substituting for L_s from equation (5) and for s **(7)**

$$\underset{m}{\overset{\bar{L}}{}}\frac{1}{2}(y')^2 \quad ' \quad (P_o \ \& \ P)\frac{\bar{L}}{EA} \quad \% \ (P_o \ \& \ P)^2/(EA\mu p\pi d)$$

The solutions to this quadratic in (P_o-P) for the various localised modes lead to a series of relationships similar to equation (4). The details and, more usefully, the results are given in Hobbs (1984) and Hobbs and Liang (1989), and re-presented here recognising the correspondence (i) between w in Hobbs and Liang (1989) and $\mu p\pi d$ here, and (ii) between $\mu_L w$ for modes 1-4 in Hobbs and Liang (1989), or φw for the 4 mode in Hobbs (1984) and pd here.

For the 4 mode:

$$P \quad ' \quad 4\pi^2 EI/L^2 \tag{8}$$

$$P_o \quad ' \quad P \ \% \ 4.7050 \ \text{x} \ 10^{\&5} \ AE(pd/EI)^2 \ L^6 \tag{9}$$

The maximum amplitude of the buckle

$$\hat{y} \quad ' \quad 4.4495 \ \text{x} \ 10^{\&3} \ \frac{pd}{EI} \ L^4 \tag{10}$$

and the maximum bending moment

$$\hat{M} \quad ' \quad 0.05066 \ pd \ L^2 \tag{11}$$

while the maximum slope

$$\hat{y}' \quad ' \quad 0.01267 \ pdL^3/EI \tag{12}$$

The results for modes 1-4 can be presented in a common format. Taking the half-wavelength of the most significant part of the buckle as L in each case (Fig.4), and using the constants of Table I, the reduced axial force within the buckle is given by

$$P \quad ' \quad k_1\frac{EI}{L^2} \tag{13}$$

Then

$$P_o \ ' \ P \ \% \ k_3 \mu p \pi d L \left[\left(1 \ \% \ k_2 \ \frac{AEpdL^5}{\mu\pi(EI)^2} \right)^{0.5} \& 1 \right] \tag{14}$$

The maximum amplitude of the buckle

$$\hat{y} \ ' \ k_4 \ pdL^4/EI \tag{15}$$

while the maximum moment

$$\hat{M} \ ' \ k_5 \ pd \ L^2 \tag{16}$$

Table I
Constants for Lateral Buckling Modes

Mode	Constants				
	k_1	k_2	k_3	k_4	k_5
1	80.76	6.391×10^{-5}	0.5	2.407×10^{-3}	0.06938
2	$4\pi^2$	1.743×10^{-4}	1.0	5.532×10^{-2}	0.1088
3	34.06	1.668×10^{-4}	1.294	1.032×10^{-2}	0.1434
4	28.20	2.144×10^{-4}	1.608	1.047×10^{-2}	0.1483
4	$4\pi^2$	4.7050×10^{-5}		4.4495×10^{-3}	0.05066

2.3 Plastic Buckling

2.3.1 Infinite mode

As noted earlier, it is assumed that elastic buckling defines the shape from which plastic buckling grows. In particular, the buckle length at which the first plastic hinge forms in the various modes can be determined from equation (11) for the 4 mode, or equation (16) for modes 1-4 by putting

$$\hat{M} \ ' \ M_p \ ' \ k_5 \ pd \ L^2 \tag{17}$$

where M_p is the fully plastic moment (hinge moment) for the buckling element. Assuming that such a moment can be calculated for a bundle of filaments, equation (17) defines the buckle length in the various modes at the onset of plasticity. Given this value of L, denoted L_p to flag the onset of plasticity, equations (8)-(10) for the 4 mode, and (13)-(15) for modes 1-4 then define the maximum amplitude, $\hat{y}_p$, the force in the buckle, P_p, and the axial force remote from the buckle, P_{op}, all at the onset of plasticity as the subscript indicates.

Concentrating first on the periodic 4 mode, it is assumed that following the onset of plasticity the half-wavelength remains constant at L_p, but the amplitude grows and the waveform changes to a sawtooth form (Fig.5) because the curvature is concentrated at the hinges.

If the (small) slope of the incremental displacement "sawtooth" is θ, the amplitude (Fig.5) grows from $\hat{y}_p$ to

$$\hat{y} ' \hat{y}_p \% 0.5 L_p \theta \tag{18}$$

Since the maximum moment in the elastic curve is M_p and remains constant as the plastic "mechanism" develops, then

$$M_p ' P_p \hat{y}_p ' P(\hat{y}_p \% 0.5 L_p \theta) \tag{19}$$

It might be noted that the lateral force per unit length, pd, does not appear in equation (19) because it cancels.

Equation (19) may be rearranged to give

$$P ' P_p \hat{y}_p \, /(\hat{y}_p \% 0.5 L_p \theta) \tag{20}$$

In essence, because the amplitude grows while the moment remains constant, the axial load in the buckle must fall.

A second condition exploits the idea of displacement compatibility which was so important in the elastic analysis. Just before the onset of plasticity, the force in the buckle is P_p, which is less than the prebuckling force P_{op}, so that the length L_p must have extended by

$$(P_{op} \& P_p) \, L_p \, /EA ' e_p, \, say \tag{21}$$

It is also worth recalling that this extension matches the arc length term

$$\int_0^L 0.5(y')^2$$

The extension, or "endo", changes as the plastic buckle develops and the force changes to P, with which is associated a prebuckling force P_o. (P_o is none too easy to visualise in the 4

mode, but in modes 1-4 is the force in the beam well away from the plastic buckle). The new value of e is

$$e ' (P_o \& P) L_p /EA \tag{22}$$

The *change* in endo, e-e_p, is associated with additional "arc length" effects, which are easy to evaluate for the sawtooth incremental form of Fig.5:

$$\Delta e ' e\&e_p ' 2\left(\frac{L_p}{2} (1\&\cos\theta)\right) ' L_p\theta^2/2 \tag{23}$$

for small θ. Substituting for e and e_p, and rearranging

$$(P_o \& P) \& (P_{op} \& P_p) ' EA\theta^2/2 \tag{24}$$

or

$$P_o ' P \% (P_{op} \& P_p) \% EA\theta^2/2 \tag{25}$$

Equations (20) and (25) are of practical use, taken with equation (18). Equation (20) defines P as a function of θ, and equation (25) gives $P_o(\theta)$. Equation (18) allows the results to be plotted as a function of the peak amplitude of the buckle, a parameter which can also be used, Hobbs (1984), to present the elastic results.

2.3.2   Modes 1-4

The approach is to combine the ideas developed for the mode 4 plastic buckling, and the concepts employed in treating the elastic buckling modes 1-4.

To make progress, it is necessary to make some assumptions concerning the likely incremental geometry of the various plastic buckling modes. The first assumption is that the plastic buckle lengths are similar to the elastic ones, and the second group of assumptions concern the number and location of hinges in the collapse mechanisms (Fig.6), and some other geometric details such as the amplitude ratio in mode 4.

With these assumptions, it is possible to find, for each mode:

(i)   equations defining the buckle amplitude analogous to equation (18);
(ii)   equations analogous to equation (20) for the reduced value of P in the plastic buckle;
(iii)   equations analogous to equation (23) for Δe leading to results comparable to a combination of equations (14) and (25) for the force P_o remote from the buckle.

In detail, then, the amplitudes are given by

$$\hat{y} \ ' \ \hat{y}_p \ \% \ c_3 \ L_p \ \theta \tag{26}$$

and the force P by

$$P \ ' \ P_p \hat{y}_p / \hat{y} \ ' \ P_p \hat{y}_p / (\hat{y}_p \ \% \ c_3 L_p \theta) \tag{27}$$

where c_3 is a constant given in Table II for the various modes.

The changes in arc length are

$$\Delta e \ ' \ c_1 L_p \theta^2 \tag{28}$$

where the coefficients c_1 are also given in Table II.

As the plastic buckle forms, three effects are apparent:

(i)   the load in the buckle drops from P_p to P, while the equilibrium value of the force remote from the buckle falls from $\bar{P}_{op}$ to P_o;
(ii) e increases by Δe (equation (28));
(iii)   the slip into the buckle increases by Δs each side or $2\Delta s$ in total, where

$$2\Delta s \ ' \ 2(s \& s_p) \ ' \ \left((P_o \& P)^2 \ \& \ (P_{op} \& P_p)^2 \right) / (EA \mu p \pi d) \tag{29}$$

The incremental compatibility condition then becomes

$$\Delta e \ ' \ 2\Delta s \ \% \ (P_p \& P) \bar{L}_p / EA \tag{30}$$

where the second term on the right hand side represents the incremental extension of the whole buckle as it develops plastically.

Taking mode 3 as an example:

$$\Delta e \ ' \ 0.983 \ L_p \theta^2,$$

$$\bar{L}_p \ ' \ 2k_3 L_p \ ' \ 2.588 L_p$$

$$P \ ' \ P_p \hat{y}_p / (\hat{y}_p \ \% \ 0.5 L_p \theta)$$

Substituting these results and equation (29) into equation (30) and rearranging, P_o is found as a function of θ

$$P_o \ ' \ P \ \% \left[(P_{op} \& P_p)^2 \ \% \ 0.983 L_p \theta^2 EA \mu p \pi d \ \& \ 2.588 L_p (P_P \& P) \mu p \pi d \right]^{0.5} \tag{31}$$

In general, for modes 1-4:

$$P_o \ ' \ P \ \% \left[(P_{op} \& P_p)^2 \ \% \ c_1 L_p \theta^2 EA \mu p \pi d \ \& \ c_2 L_p (P_p \& P) \mu p \pi d\right]^{0.5} \tag{32}$$

where the constants c_1 and c_2 are given in Table II.

Table II
Constants for plastic lateral buckling

Mode	Constants		
	c_1	$c_2 = 2k_3$	c_3
1	0.35	1	0.35
2	0.608	2	0.346
3	0.983	2.588	0.5
4	0.830	3.216	0.4

Operationally, for each mode equation (27) defines P as a function of θ, and equation (32) then gives $P_o(\theta)$. Equation (26) allows the results to be plotted as a function of the amplitude of the buckle, $\hat{y}$.

3. APPLICATION OF MODEL

3.1 Role of imperfections

The general form of the results of the foregoing analysis is summarised in Fig. 7, together with a schematic presentation of the effects of various imperfections in rope lay up. The figure shows plots of buckle amplitude against the axial compressive load on a rope component at a position remote from the buckle.

Fig. 7(a) focuses on the purely elastic behaviour, and is indicative of the phenomena encountered in any of the localised modes, Modes 1-4, which are of greater practical importance than the infinite mode. Using equations (14) and (15), the upper curve is the locus of force and amplitude in an initially perfectly straight rope element in static equilibrium, an "equilibrium path". The descending part of this curve, from A to B, consists of points in unstable equilibrium, while the rising part of the curve is stable. The consequence is that if a perfect system were brought by some means to a point such as A and released it would not stay put, but would instead snap dynamically to some position with a much greater amplitude and wavelength such as C. It is not easy to visualise just how a perfectly straight rope element might be made, still less taken up to point A, but in the classical literature in this field it was widely thought that the minimum of curve AC, point B, represented a force below which buckling could not occur in a perfect axially loaded element. The lowest minimum for modes 1-4 was for some time regarded as a "safe load" (or in thermally loaded

beams, equivalently, as a "safe temperature") for use in design with an appropriate safety margin.

However, once engineers began to address the effects of the initial imperfections which are inevitably present in real railway tracks and pipelines, it rapidly became clear that the "safe temperature" was a potentially dangerous illusion. This may be seen from the three curves from D_1, D_2, D_3 in Fig. 7(a), where the effects of three different initial amplitudes of buckles, or irregularities, are sketched. All of them erode the "safe load" at B to some extent. The first curve indicates the consequences of a small initial misalignment: a curve rising from D_1 to a peak at E before falling to a minimum below B before rising again to meet the perfect curve asymptotically near C. The falling part of this curve, too, is unstable, so that an imperfect beam subjected to a load gradually increasing from zero would only follow path D_1 as far as E before suddenly losing stability and snapping to F on the rising part of the curve. Larger imperfections D_2 and D_3 show respectively a smaller snap at a lower load, and a monotonic (albeit nonlinear) rising behaviour. At large enough amplitudes all of the imperfect curves converge asymptotically to the perfect response.

It is certain that the elements of a rope are no more likely than a pipeline or railway track to be perfectly straight at zero load. As well as any imperfections in the manufacturing process, the helical lay of, say, a core strand will predispose the strand to buckle in different directions within a given lay length, while the gaps between the neighbouring strands will inevitably provide a lower radial pressure locally than the uniform radial pressure assumed in the analysis, as well as some space for the core strand to deform into. Thus even before the question of the possibility of plastic hinge formation in the strand is addressed it is clear that a strand is likely to be affected by significant initial imperfection effects in the same way as the pipelines whose analysis suggested this treatment.

Fig. 7(b) outlines some of the possibilities once the formation of plastic hinges is postulated. As the amplitude of buckles increases, so does the maximum bending curvature, which will eventually reach the plastic yield condition. In principal, depending only on the plastic yield moment of the yarn or strand under consideration, a plastic hinge could occur at the crest of a buckle at any amplitude, whether small or large. The "perfectly straight case" is represented by the lines from H_1, H_2, H_3, H_4.   The plastic responses, which are superimposed on the curve ABC from Fig. 7(a), peel off from the elastic equilibrium path and drop below it, before rising again at rather large amplitudes. It was noted above that the perfect path would snap from A in the elastic case: in the plastic case the snap would be more vigorous because it would be to a much larger amplitude than that on the elastic rising path.

The behaviour of the elasto-plastic imperfect system is illustrated in Fig. 7(b) by "snapping" from the curve D_1 of Fig. 7(a). Some interesting possibilities arise. Taking hinge formation at the first of the four amplitudes selected in the perfect case, at H_5, plasticity would develop well before E, the peak of the elastic imperfect curve, and cause a snap at once to a rather large amplitude. At this point it is worth recalling that although the amplitude grows in a plastic buckle it has been assumed in the analysis above that the wavelength, defined as it is by the hinge positions, does not change: in this it differs from the elastic analysis where amplitude growth goes hand in hand with wavelength growth.

Prediction of hinge formation at equilibrium positions like H_6, H_7, H_8 would imply that a strand under load increasing steadily from zero would first reach point E. For the cases, H_6 and H_7, it would then start to snap elastically, but, when the critical amplitude was reached would peel off the unstable dynamic buckling curve to form hinges at amplitudes H_6 and H_7, close to those of H_2 and H_3 respectively. The snap would continue at constant wavelength towards the rising part of the plastic equilibrium paths from H_6 to H_7, joining asymptotically around G. For case H_8, there would also be snap at E, but to the elastic line, which would be followed until the plastic hinge formed at H_8, close to H_4.

As noted below, buckling in rope yarns has been observed where realistic numerical values for the yarn and fibre properties seem to be consistent with the small amplitude/short half-wavelength formation of plastic hinges. A history like D_1 H_5 or D_1 E with a snap towards G at constant wavelength would provide a plausible explanation for the observed condition of the yarns.

It is recognised that much of the above discussion is heuristic, but it appears to cast light on phenomena which have been the subject of much debate among the authors. Without information on the nature of imperfections - and a more complicated theory - it is not possible to make a prediction of the response based on independent input data. However, the plastic deformation equations can be solved if an arbitrary choice of the amplitude, and hence also the half-wavelength and slip length, of buckles is made.

3.2 Numerical calculation

A computer program has been written to determine solutions to the equations. Calculations applicable to an aramid (Twaron 1000) rope, for which experimental observations are given in the next section, have been carried out. This rope was tested in tension-tension cycling at $38 \pm 24\%$ break load. The rope has a "wire-rope construction" with 6 strands round a single core strand. Each strand is composed of 6-round-1 rope yarns. The core rope yarns in each strand contain 7 "textile" yarns, as supplied by the fibre manufacturer; the outer rope yarns in each strand contain 5 "textile" yarns. The calculations relate to the core rope yarn of the core strand. The relevant parameters in SI units, with conversions in brackets are as follows. The symbols relate to the rope yarn, which is the basis for the calculation, and the values used in the computation are put in **bold**.

FIBRE: linear density = 1.7E-7 (1.7 dtex); density = 1.44E3 (1.44 g/cm^3); area = 1.7E-7/1.44E3 = 1.18E-10 (1.18 x 10^{-4} mm^2); diameter = $/$ (4A/π) = $/$ (4 x 1.18E-10 / 3.142) = 1.226E-5 (12.26 μm).

"TEXTILE" YARN: 1000 fibres; linear density = 1.7E-4 (1700 dtex); total fibre area = 1.18E-7 (0.118 mm^2); diameter of equivalent solid rod = $/$ (4 x 1.18E-7 / 3.142) = 3.876E-4 (0.3876 mm). Assume packing factor = 0.7: area = 1.68E-7 (0.168 mm^2); diameter = $/$ (4 x 1.68E-7 / 3.142) = 4.625E-4 (0.46 mm).

ROPE YARN (strand core): 7 "textile" yarns; linear density = 1.19E-3 (1190 tex); total fibre area = 8.26E-7 (0.826 mm^2); diameter of equivalent solid rod = 1.03E-3 (1.03 mm). Assuming packing factor = 0.67: area A = **1.23E-6 (1.23 mm^2)**; diameter d = $/$ (4 x 1.23E-6 /

3.142) = **1.25E-3 (1.25 mm)**, which was the measured diameter.

ROPE: number of "textile" yarns = (7 x 7) in strand cores + (7 x 6 x 5) in strand outers = 259; total fibre area = 3.05E-5 (30.5 mm^2). Assume packing factor of 0.635: area = 4.80E-5; diameter = $\sqrt{}$ (4 x 4.80E-5 / 3.142) = 7.82E-3 (7.82 mm), which was the measured diameter.

MECHANICAL PROPERTIES: fibre modulus = 7.8E10 (78 GPa); for packing factor of 0.67, yarn modulus E = **5.23E10 (52.3 GPa)**.
Fibre yield stress = 5E8 (0.5 GPa); this is the value given by van der Zwaag and Kampschoer (1987) for Twaron; Allen (1987) gives 0.37 GPa for Kevlar. Yarn yield stress (corrected for packing) f_y = **3.35E8 (0.335 GPa)**.
Coefficient of friction μ = **0.15**; measurements in FIBRE TETHERS 2000 (1995) gave values between 0.12 and 0.19.

RADIAL PRESSURE: p = **1E8 (0.1 GPa)**. The minimum tension in the fatigue testing was 14% of break load. The rope has a nominal break load of 5 tonne (50 kN), which, since it contains 259 yarns, would give a tensile strength of approximately 1.15 GPa and a minimum tensile stress on the rope of approximately 0.16 GPa. This implies that the radial pressure would equal 63% of the tensile stress. Calculations carried out using a computer program OP*TTI*-ROPE from TTI Ltd gave values of radial pressure between 0.07 and 0.18 Gpa.

Although there is uncertainty in some of the above values, the major problem is in deciding the values to take for the bending stiffness and the plastic bending moment of the yarn. These quantities depend on the frictional interaction between fibres in the yarn, and may change as a buckle develops and the stresses in the rope change. One extreme is that the yarn acts as a solid rod. The other extreme to be considered is a yarn with free sliding between fibres. This case assumes no frictional interaction between fibres, but has cooperative buckling of individual filaments so that the lateral and axial restraints in the model would act on the yarn as a whole. The experimental observations indicate that it is rope yarns that buckle, and this is assumed in the following calculations. Other options would be buckling and slipping of strands, "textile" yarns, or, most unlikely of all, individual fibres.

As noted above, there are two bounds to the bending stiffness and the plastic moment values, with the expectation that the truth will lie somewhere between these limits. Consider the bending rigidity EI first. The upper limit, the solid rod, has a second moment of area, $I = \pi d^4 / 64$ where d is again the yarn diameter, and the influence of the voids between individual fibres is accounted for by reducing Young's Modulus from the fibre value to the yarn value of 52.3GPa. The lower limit is simply the second moment of area of an individual fibre, multiplied by the number of fibres in the yarn. This value should be multiplied by the fibre modulus to produce the correct value of the bending rigidity EI. In practice, to avoid having to input both the fibre and yarn moduli separately, the value of I calculated here was scaled up by dividing it by the packing fraction and the correct EI produced by using the *yarn* modulus. Thus the limits on I used here were:

SOLID ROD: Second moment of area I = 1.20E-13 (**0.120** mm^4); EI = 6276 Nmm^2

FREE SLIDING FIBRES: Second moment of area I = 7.76E-18 / 0.67 (**11.58E-6** mm^4); EI =

0.606 Nmm^2

Turning to the calculation of the limits on the fully plastic moment of the rope yarn, it has been noted that the fibre yield stress in compression (0.5 GPa) is very much smaller than that in tension. As yielding develops this means that the bending neutral axis shifts towards the tension side of the fibre and at the limit a very small tension area at very high stress balances the rest of the fibre cross section which is yielding in compression. Simple statics then suggests that the fully plastic moment of the fibre is $r^3 f_y$, where r is the fibre radius, and the fully plastic moment of the bundle of N fibres is just:

$$M_p = N \; r^3 f_y \qquad\qquad\qquad (33)$$

At the other, solid rod, limit the same concept is exploited (rather speculatively) with the yield stress reduced to the yarn value of 0.335 GPa to give:

$$M_p = d^3 f_y / 8 \qquad\qquad\qquad (34)$$

where d is now the yarn diameter.

Substituting the values quoted earlier, the plastic moment limits are:

SOLID ROD. M$_p$ = 2.57E-1 Nm (**257** Nmm)

FREE SLIDING FIBRES. M$_p$ = 2.53E-3Nm (**2.53** Nmm)

It is worth noting at this point that the computer program written using the analysis presented in this paper does not input M_p directly. Rather, the values of the plastic buckle length given by substituting the limits on M_p into equation (17) were recorded (for Mode 4 the values are 3.72 mm for the solid rod and 0.369 mm for the free sliding fibres). In addition it should be recognised that the co-existing compressive force in the element at buckling will reduce the effective plastic moment. With the area of 1.23 mm^2, an axial force of 300 N will give a compressive stress of some 0.26 GPa or roughly 50% of yield, cutting M_p by the same proportion.

Substitution of the numerical values in the equations gives values of buckle length, buckle amplitude, and slip length between buckles. The dimensional quantities are known to a good approximation, and a sensitivity analysis shows that only small changes are introduced by varying the modulus E, the coefficient of friction μ, or the radial pressure p by factors of two either way. Large changes come from the big differences in bending properties.

Figures 8 (a) and 8(b)show the solutions for the mode 4, perfect, elastic and elasto-plastic buckling for the solid rod and the free sliding of fibres in the rope yarn. Values of the buckle amplitude, buckle length and slip length at the elastic minimum point B are given in Table III.

Table III
Predictions for mode 4, perfect elastic buckling.

At point B	Solid rod	Free sliding
buckle amplitude(mm)	1.22	0.0165
half-wavelength(mm)	8.75	0.296
slip length(mm)	19.70	1.84

We next consider the departure of the plastic curve from the elastic curve. For the solid rod, the plastic buckle length is **[3.72]** mm, which is less than the value of **[8.75]** mm at the elastic minimum. This causes the computer program to produce the square root of a negative quantity, suggesting that plastic buckling would not occur in the "perfect" case. However, this is not a problem when imperfections are present, as described in the previous section. Since the departure in the imperfect case may occur at various lengths, it was arbitrarily assumed that plasticity might occur at buckle lengths of **[8.75]** (equal to the elastic minimum), **[7.5]** or **[10.0]** mm. For the free-sliding buckling, the elastic minimum is at **[0.296]** mm, and the calculations have also been made for **[0.25]** and **[0.350]** mm. The results of the calculations are shown in Table IV. Other values of *EI* are selected for intermediate cases between the solid rod and free sliding, as shown in the lower part of Table IV. The buckle lengths are at the elastic minima. The results cover a wide range, due to the uncertainties in the bending behaviour of yarn subject to lateral pressure and to the arbitrary choice of buckle length. However they are qualitatively compatible with a response which matches the observed values given in the next section.

Table IV
Predictions for mode 4, elasto-plastic buckling

	SOLID ROD CASE			FREE SLIDING CASE		
EI, M_p =	6276 Nmm^2, 257 Nmm			0.606 Nmm^2, 2.53 Nmm		
half wave-length (mm)	8.75	7.5	10	0.296	0.25	0.35
buckle amplitude (mm)	1.87	1.62	2.8	0.027	0.014	0.044
slip length (mm)	19.7	9.52	35.5	1.84	0.92	3.55
INTERMEDIATE CASES	$EI = 627$		$EI = 62.7$		$EI = 6.27$	
half-wavelength (mm)	3.56		1.62		0.653	
buckle amplitude(mm)	0.534		0.228		0.065	
slip length (mm)	8.65		6.14		2.72	

3.3 Sensitivity

The results in the previous section show the major influence of the bending properties on the buckling response. As slip develops radially inwards at an incipient hinge in the solid rod, the effective second moment of area will fall progressively. It might be expected that at some point the buckle wavelength will "gel" (in cooperation with the imperfections which are

present) and a full hinge will form at constant buckle length. The range of buckle lengths between the solid rod and cooperating fibre limits certainly includes those found in the tests, described below.

In addition, although the uncertainty in the bending stiffness does place limitations on the quantitative use of the present analysis, it is still useful to indicate the effects of changes in the other parameters involved. Table V gives results (for the two limiting cases of the bending properties) which indicate the influences of halving (one at a time) Young's modulus, E, the radial pressure, p, and the friction coefficient, μ. Perhaps the most interesting effect revealed by this parametric study is the large influence of the friction coefficient on the slip length and hence the minimum gap between buckle groups, which is (as noted earlier) twice the slip length.

Table V
Sensitivity predictions: values changed from standard in bold type

INPUT VALUES	SOLID ROD CASE				FREE SLIDING CASE			
E (GPa)	52.3	**26.2**	52.3	52.3	52.3	**26.2**	52.3	52.3
p (GPa)	0.1	0.1	**0.05**	0.1	0.1	0.1	**0.05**	0.1
μ	0.15	0.15	0.15	**0.075**	0.15	0.15	0.15	**0.075**
CALCULATED								
half -wave length (mm)	8.75	6.76	10.19	8.98	0.296	0.253	0.346	0.307
buckle amplitude (mm)	1.85	1.63	1.77	2.18	0.027	0.028	0.027	0.033
slip length (mm)	19.7	9.79	24.1	35.3	1.84	1.48	2.27	3.18

4. OBSERVATIONS OF KINKING

In the joint industry study, FIBRE TETHERS 2000 (1995), ropes with 5 and 120 tonne break loads were subject to tension-tension fatigue over a variety of ranges. The ropes were made in several different constructions from aramid, HMPE, LCP and polyester fibres. When cycled between a higher tension and low enough values of minimum load, there was evidence of axial compression fatigue. By marking the ropes with strips of adhesive tape, it was possible to observe twisting in some tests. Ropes, which were not torque-balanced but were terminated with splices, showed a cyclic rotation at the centre of the test length. This is explained by varying tension causing a varying torque, which then leads to a cyclic twisting of the rope against the low torsional resistance of the splices at each end. In some other tests, with rigid terminations, there was relative rotation in different parts of the test lengths due to rope variability. Another cause of axial compression is a difference in component lengths. Axial compression in one rope was attributed to tension in a braided jacket. The tightness of the jacket indicated a strong radial component of yarn tension. In the helical braid, the axial component of tension in the jacket yarns puts the core into compression.

A number of these ropes were examined to observe the form of damage. One technique used in studying aramid ropes was to dye the yarns with a red dye (Kodak 8314 p-

dimethylaminocinnamaldehyde). The dye is selectively absorbed into damaged regions. In typical observations, sharp red bands about 0.5 mm wide were observed crossing the yarns. Sometimes these were single bands, which would correspond to mode 1 above; in other places, there were groups of several bands, corresponding to a higher mode. The damaged areas were separated from one another by undamaged lengths of yarn, qualitatively in accord with the theoretical predictions.

Rope samples were also studied by visual examination, photography, optical microscopy and scanning electron microscopy. A few examples will be shown here, but a larger selection of the observations are reported by Hearle et al (1998).

The Twaron rope specified in section 3.2, which was cycled at 38$\pm$24% break load with resin socket terminations, failed after 173,950 cycles. The core rope yarn of the core strand had many breaks distributed over the entire length. Unbroken portions of other yarns retained between 72.5 and 84.3% of their strength, but some individual break values were as low as 63% strength retention. Thus the failure is compatible with break at the peak load of 62% of new break load. Figure 9 shows the core yarn of the core strand broken into short pieces, between about 3 and 15 mm long, and long pieces, between about 70 and 150 mm long. The pieces at about 150 mm length show an unbroken buckle at the mid-point, so that the slip length is about 70mm. These lengths correspond to the half-wavelengths and slip lengths computed in the previous section.

An HMPE (Dyneema) rope in a similar construction was unfailed after a million cycles at 20$\pm$19.5% break load with resin socket terminations. Despite the very low minimum load (0.5% of break load), this longer life could be attributed to a combination of lower peak load, higher resistance to axial compression fatigue in HMPE, and the fact that this must have been a well-made rope in a rigid termination. Nevertheless, all the yarns showed evidence of buckling. Fig. 10(a) shows groups of buckles at intervals along all the yarns of an outer strand, which retained between 40 and 95% of new strength. Fig. 10(b) shows buckles in the outer yarns of the core strand and breaks in the centre yarn.

From the UMIST SEM studies, which are reported in greater detail in Hearle et al (1998), Fig. 11 (a) shows the appearance of an aramid fibre extracted from the same Twaron rope as specified above, but cycled at 40$\pm$20% break load for one million cycles. Although the rope had not failed, some yarn breaks had occurred. The appearance at the unbroken end is similar to that shown at the end of the sets of predicted buckle forms in Fig. 6. The next more severe bend has broken. Figure 11(b) shows a Twaron fibre from a parallel yarn rope cycled at 40$\pm$25% break load without failing after one million cycles. The higher magnification shows up the internal kink bands within the fibre at the gross kinks in the fibre as a whole.

A comprehensive and explicit quantitative recording of the buckle parameters was not carried out in FIBRE TETHERS 2000 (1995). However the above ranges of 3 to 15 mm for the half-wavelength and 35 to 70 mm for the slip length are typical of what was seen. Some of the buckling appeared to be mode 1, but other examples had up to ten or more buckles in a group. Comparison with the predicted values in Tables IV and V suggest that the yarns tend towards the solid rod case, which is not surprising in view of the lateral pressures.

5.0   CONCLUSIONS

The analysis of kinking presented here facilitates a treatment of restrained buckling within

ropes and other fibre assemblies. In tension members, axial compression occurs when some components are under axial compressive loading, even though the whole assembly is under tension. In other situations, such as treading on carpets, the loading action may put the whole of a localised part of the assembly into compression, but within a constrained surrounding of other yarns. Because oriented fibres have low compressive yield stress, which causes a low plastic bending moment, the buckling results in sharp kinks, which fail after repeated cycling.

The model, which follows earlier treatments of elastic buckling in pipelines, predicts that groups of saw-tooth buckles will be separated by straight slip lengths. The forces involved are the axial compressive load, the frictional resistance to axial slip, and the lateral restraint of radial pressure. The yarn modulus and the friction coefficient have a role in determining the displacement in the slip zone, which affects the axial compressive force, but the dominant yarn properties are the bending stiffness, which sets the pattern of initial elastic buckling, and the bending yield moment, which determines the formation of plastic hinges. Unfortunately, there is a wide range of possible values for these quantities, depending on the ease with which fibres can slide over one another in the yarns. The extremes range from that for the yarn acting as a solid rod to the sum of the bending of the individual fibres. There is also uncertainty about the numerical values of some controlling parameters and about some features of the model, such as the role of imperfections and the way in which the lateral pressure operates.

While the analysis could be refined, its present accuracy may be close to the accuracy with which systems can be defined, and it is debatable where further efforts could best be focussed - on analytic refinements or the acquisition of better data. Nonetheless, the present model does reproduce the experimentally observed pattern of groups of closely spaced kinks separated by undamaged areas which have unloaded into the adjacent buckle zones. Although the observed values of 3 to 15 mm for the half-wavelength and 35 to 70 mm for the slip length are not entirely within the ranges of 0.25 to 10 mm and 1 to 35 mm respectively for the predictions in Tables IV and V, the calculated sensitivities are such that it would not be difficult to find a set of parameters to fit any observed results.

REFERENCES

Allen, S. J., 1987. Tensile recoil measurements of compressive strength for polymeric high performance fibres, *J. Materials Sci*. **22**, 853-859.

Fibre Tethers 2000, 1995. *High Technology Fibres for Deepwater Tethers and Moorings.* Noble Denton Europe Ltd, London, England.

Hearle, J.W.S., Lomas, B., and Cooke, W.D., 1998. *An Atlas of Fibre Fracture and Damage to Textiles*, Woodhead Publishing Company, Cambridge, England.

Hearle, J.W.S., and Miraftab, M., 1991. The Flex Fatigue of Polyamide and Polyester Fibres. Part 1: The Influence of Temperature and Humidity, *J. Materials Sci., * **26**, 2861-2867.

Hearle, J.W.S., and Wong, B.S., 1977. Flexural Fatigue and Surface Abrasion of Kevlar-29 and Other High-modulus Fibres, *J. Materials Sci*. **12**, 2447-2455.

Hobbs, R.E., 1984. In-service Buckling of Heated Pipelines, *ASCE, J. Transportation*

Engineering, **110,** 175-189.

Hobbs, R.E., and Liang, F., 1989. Thermal Buckling of Pipelines Close to Restraints, *8th International Conference on Offshore Mechanics and Arctic Engineering*, The Hague, March 1989, Vol. 5, pages 121-127.

Riewald, P.G., 1986. Performance Analysis of an Aramid Mooring Line, *18th Annual OTC*, Houston, Texas, May 1986, paper OTC 5187.

Riewald, P.G., Walden, R.G., Whitehill, A.S., and Koralek, A.S., 1986. Design and Deployment Parameters Affecting the Survivability of Stranded Aramid Fibre Ropes in the Marine Environment, *IEEE OCEANS '86, Conference Proceedings,* Washington D.C., September 1986, page 284.

van der Zwaag, S., and Kampschoer, G, 1987. Paper presented at Rolduc Polymer Conference, 1987.

Nomenclature

A	cross-sectional area
c	coefficients (Table 2)
d	element diameter
E	Young's modulus
e	end shortening, "endo"
I	effective second moment of area
k	coefficients (Table 1)
L	buckle half-wavelength
ø	overall length of buckle
L_s	slip length
M	moment
m	pd/EI
n	$(P/EI)^{0.5}$
N	number of fibres in yarn
P	compressive axial load
p	radial pressure on element
s	inward slip to a buckle
x	longitudinal coordinate
y	displacement normal to x
Δ	change in quantity
μ	friction coefficient
θ	plastic mechanism angle

Subscripts

o	original, remote from buckle
p	plastic

s   slip
^   peak
N   derivative

Mode 1

Mode 2

Mode 3

Mode 4
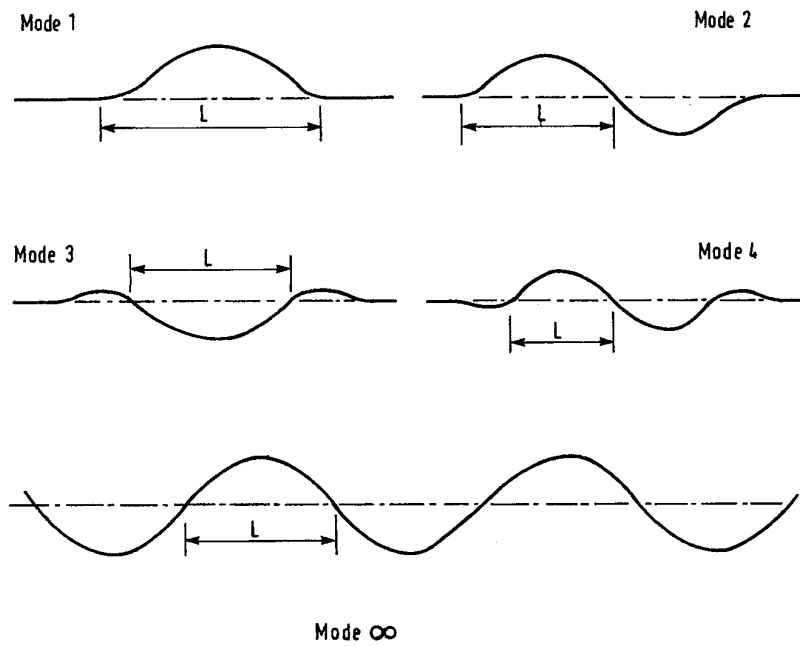
Mode ∞

Fig. 1   Periodic and localised modes

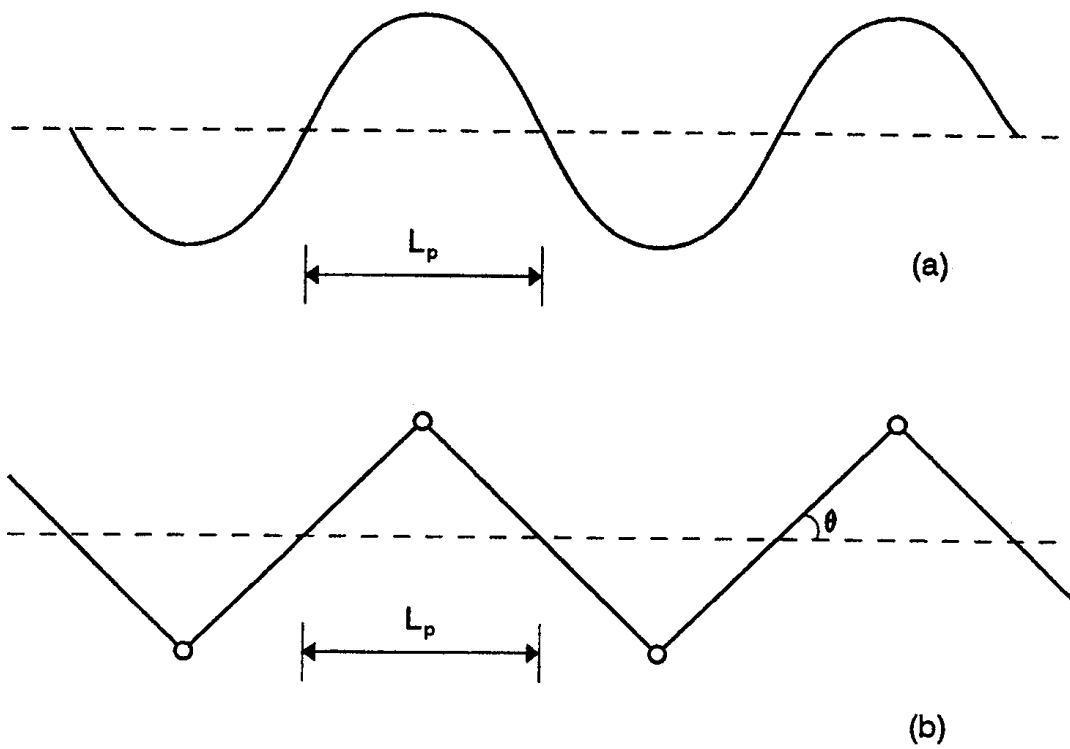**Figure 1** Periodic and localised modes
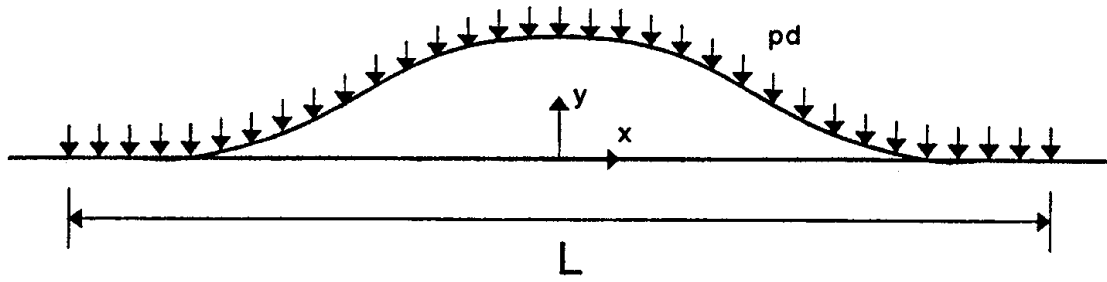
Figure 2 Details of lateral buckling
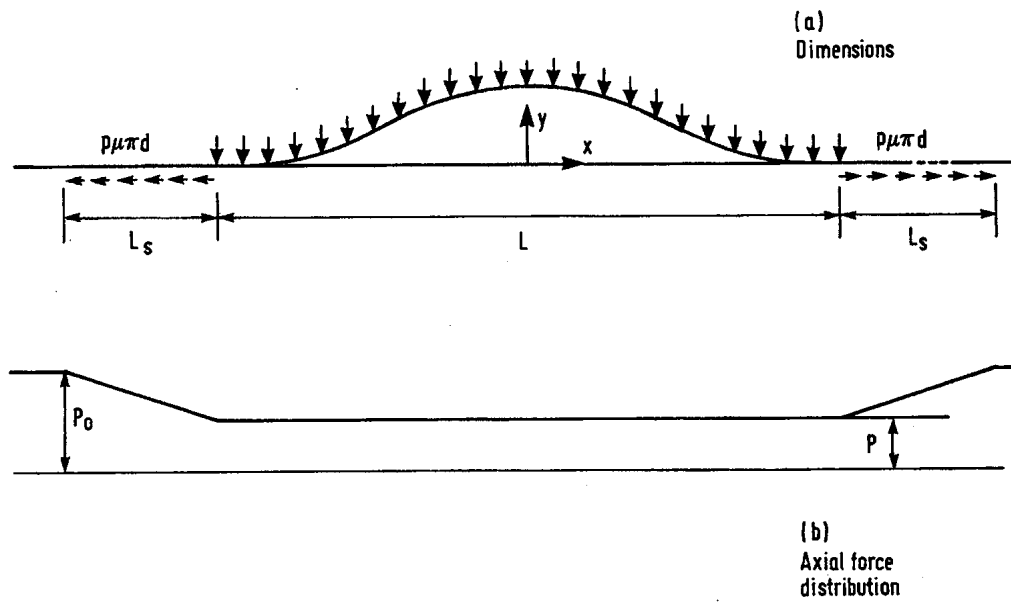
Figure 3 Slip lengths and force distribution
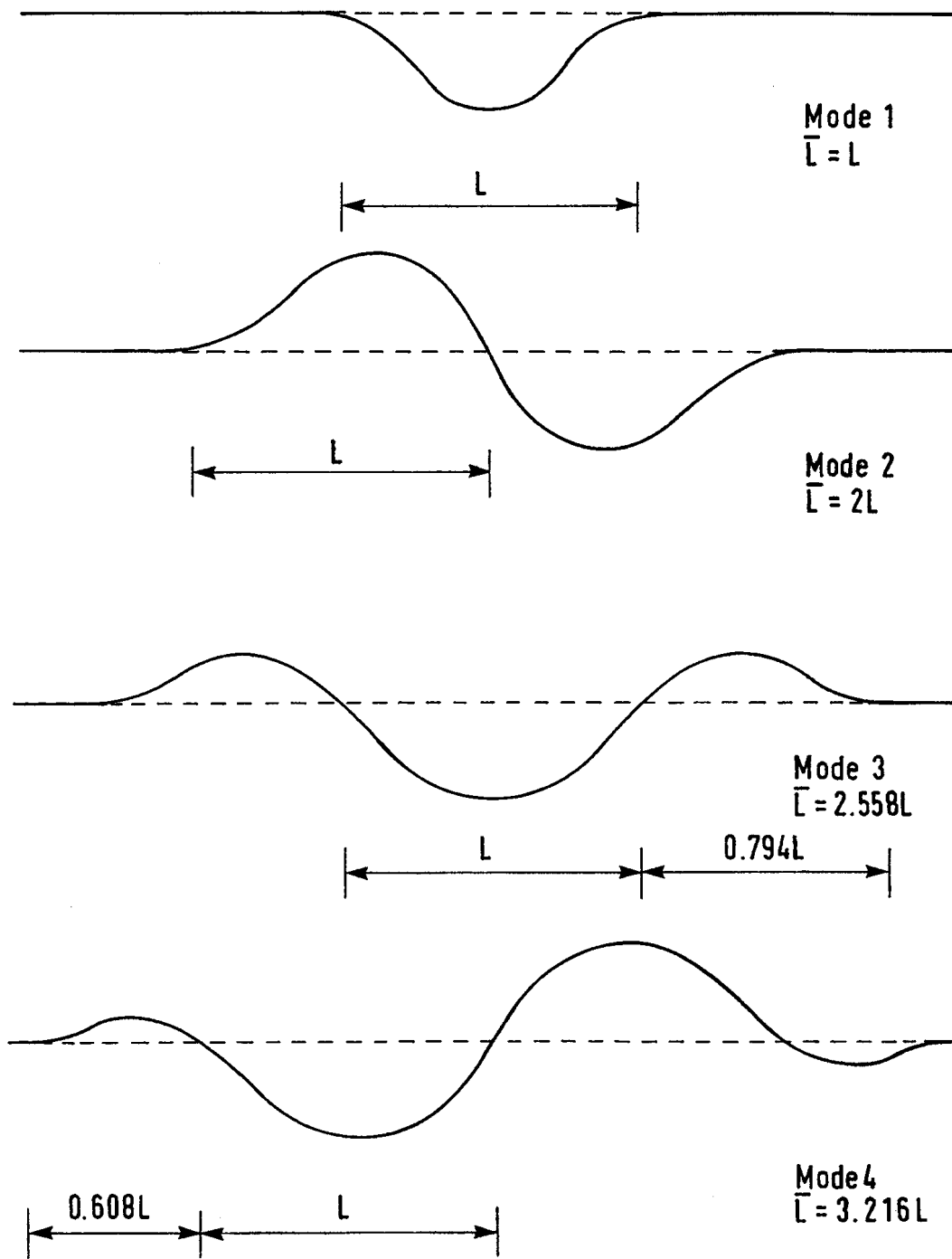
Figure 4 Geometry of elastic buckles

Figure 5 Development of elastic-plastic periodic mode: (a) at elastic limit; (b) incremental plastic mechanism
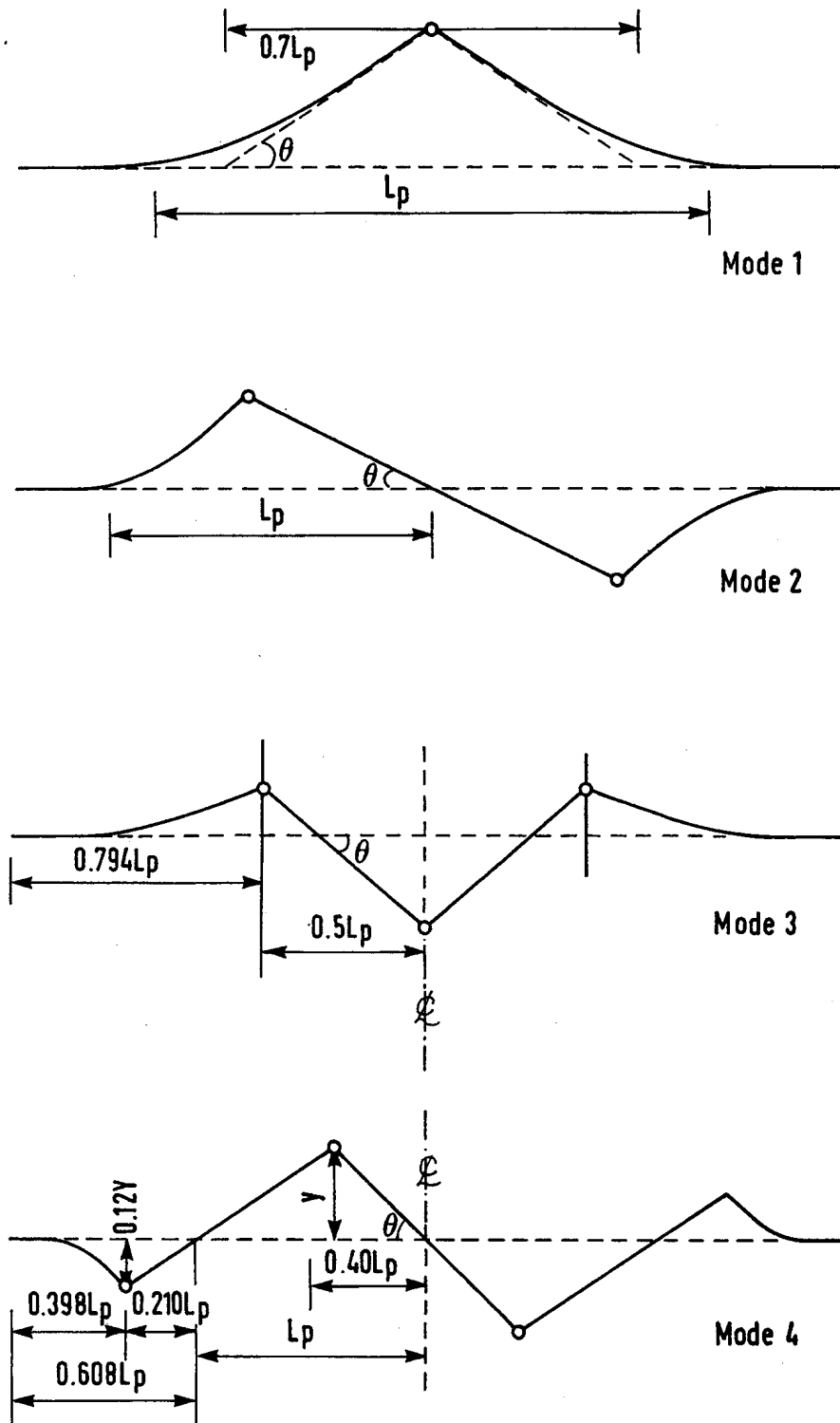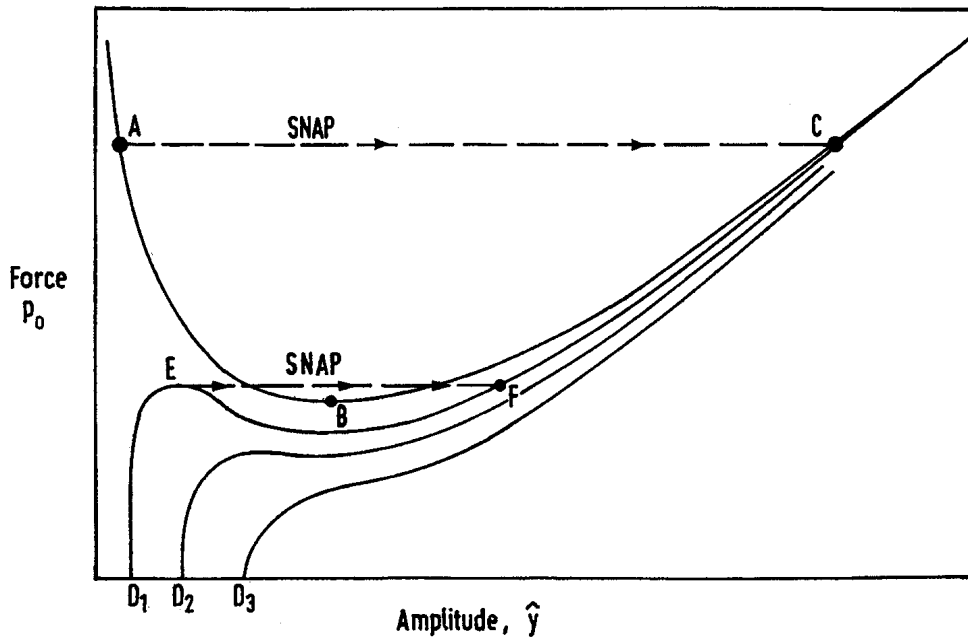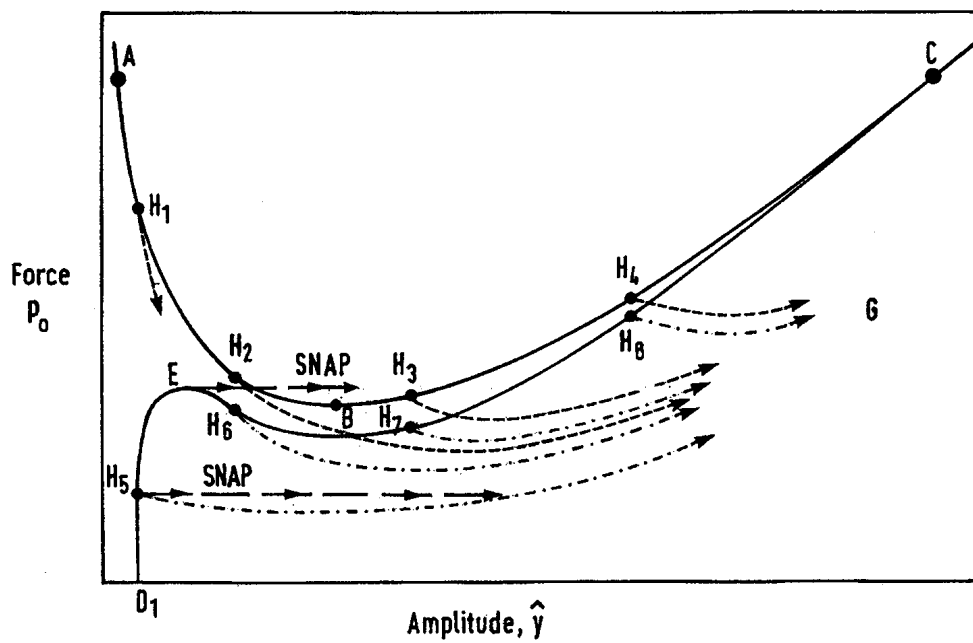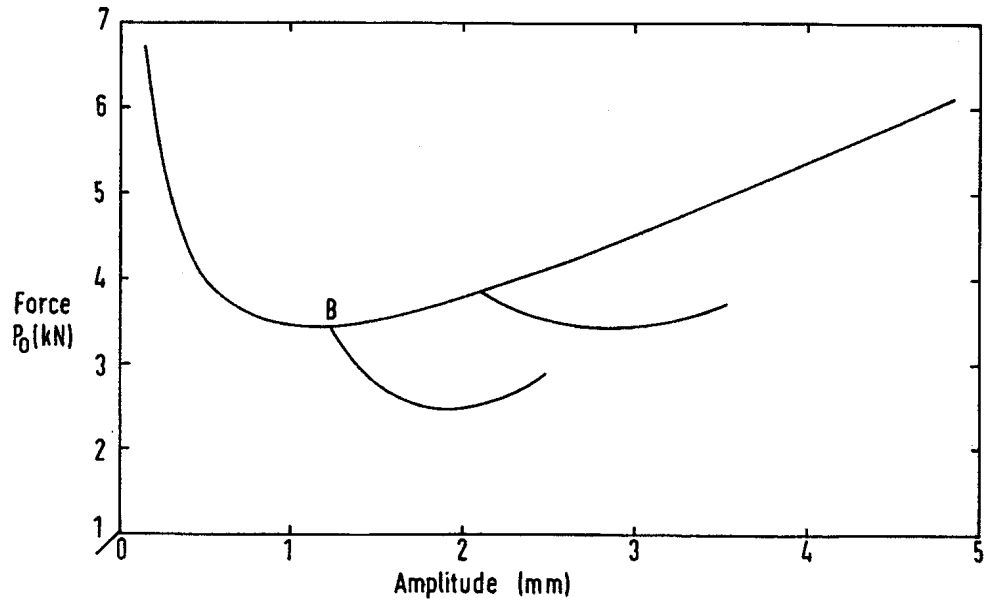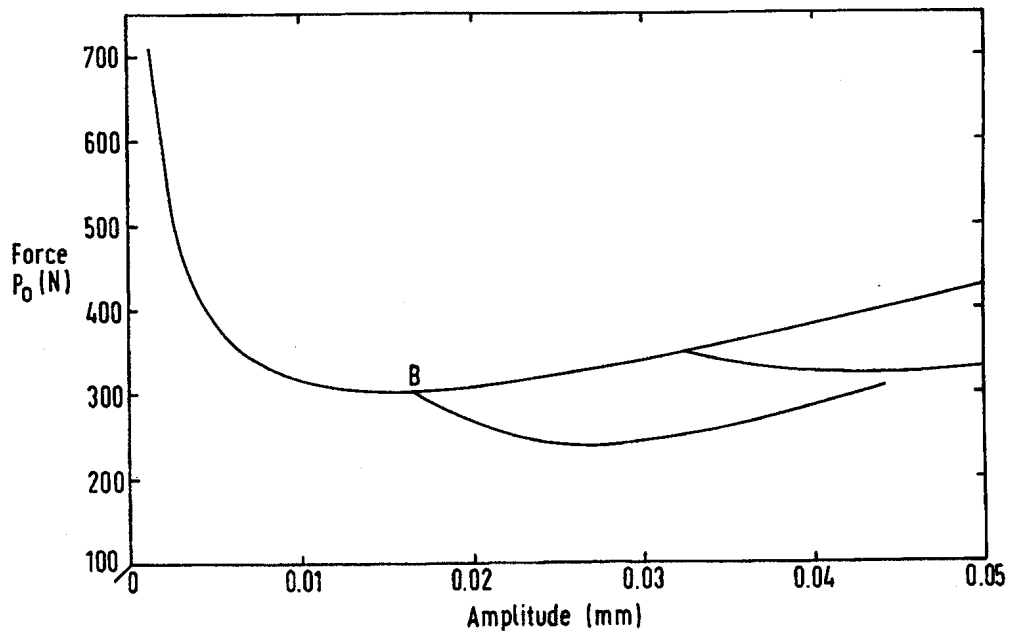
Figure 6 Geometry of plastic localised modes.

(a)

(b)

Figure 7 (a) Elastic buckling in perfect and imperfect situations. (b) Corresponding elasto-plastic buckling
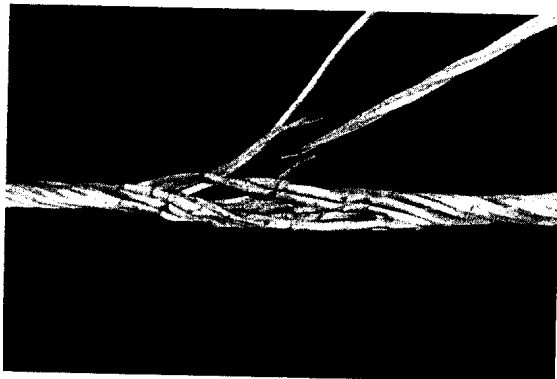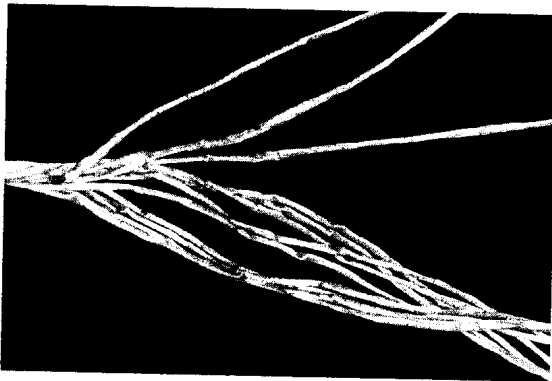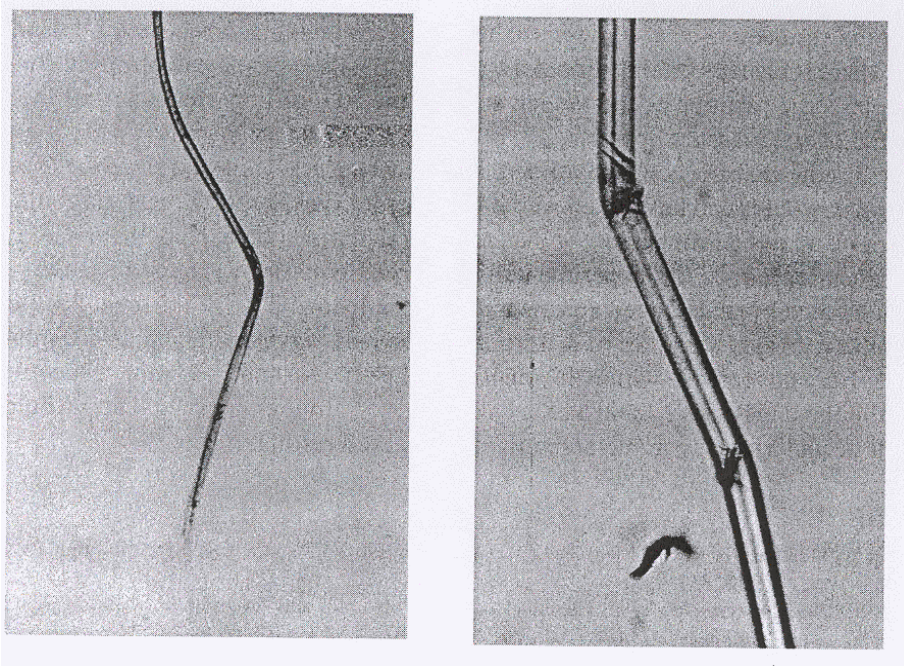
(a)

(b)

Figure 8 Predicted buckling for case specified in text: (a) solid rod; (b) free sliding
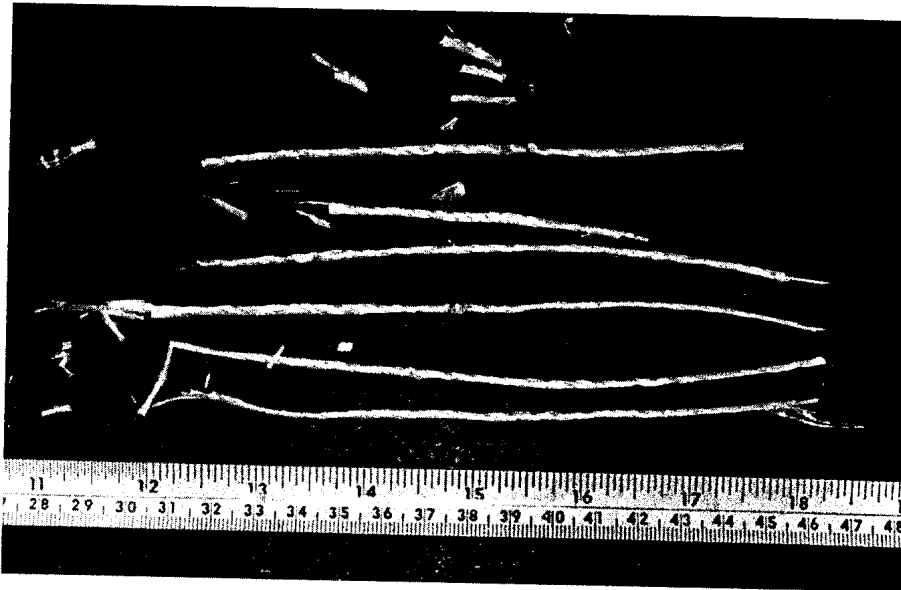
Figure 9 Core yarn of a core strand in an aramid rope after axial compression fatigue. (See details in text).

Figure 10 (a)Yarns of outer strand of an HMPE rope after tension-tension cycling. (b) Yarns of core strand. (See details in text).

Figure 11 Fibres after tension-tension cycling. (a) From aramid rope. (b) From HMPE rope. (See details in text).